Springer

Acta Mechanica Sinica

CrossMark click for updates

• RESEARCH PAPER •

Acta Mech. Sin., Vol. 39, 723044 (2023)
https://doi.org/10.1007/s10409-023-23044-x

Design of two-dimensional extremal material based on truss lattices

Kun Wang[1], Haiyu Lv[1], Xiaoning Liu[1*], Anfu Zhang[2], and Gengkai Hu[1]

[1] *School of Aerospace Engineering, Beijing Institute of Technology, Beijing 100081, China;*
[2] *Wuhan Second Ship Design and Research Institute, Wuhan 430064, China*

Received February 1, 2023; accepted March 8, 2023; published online May 22, 2023

Extremal materials with rank-deficient elastic tensor are classified by counting the soft deformation modes, while their elasticity is assigned by hard modes. To date, only pentamode materials with a single hard mode have been studied in depth, and a broader space of extremal materials is left almost unexplored. In this work, basic ingredients and design schemes aiming to more general extremal materials are studied based on truss lattices. To homogenize periodic lattices with nonaffine deformation induced by local mechanisms, we revisited the matrix formulation with singular value decomposition and derived the effective elastic tensor in compact form of Kelvin-like decomposition, with which we are able to outline the origin and design logic of extremal materials. The method is then applied to design two-dimensional extremal materials on demand of arbitrarily prescribed elasticity tensor. The unique static responses in two-dimensional unimode continua which is closely related to complex analytic functions are confirmed by our designed lattice material. The proposed method is also applicable for more general extremal materials in three-dimensional cases.

Extremal materials, Elastic tensors, Homogenization, Truss lattices, Microstructure design

Citation: K. Wang, H. Lv, X. Liu, A. Zhang, and G. Hu, Design of two-dimensional extremal material based on truss lattices, Acta Mech. Sin. **39**, 723044 (2023), https://doi.org/10.1007/s10409-023-23044-x

1. Introduction

The elastic tensor of structural materials is required to be positive definite, so that stresses are induced in response to arbitrary modes of deformation, and vice versa. However, for some materials certain eigenvalues (six for Cauchy materials in three-dimension (3D)) of the elastic tensor could be very small compared to the rest, and the corresponding eigenvectors are their soft modes. Conceptually, Milton and Cherkaev [1] named *extremal material* for this kind of materials, and proved theoretically that any positive-definite 4th order elastic tensor can be realized by properly laminating a subset of extremal materials. To the limiting case, extremal materials with rank-deficient elastic tensor are classified as unimode, bimode, trimode, quadramode and pentamode by counting the numbers of soft modes, i.e., the zero eigenvalues. Therefore, in spectrum decomposition the 4th order elastic tensor of a material with n soft modes can be expressed as

$$\mathbf{C} = \sum_{i=1}^{6-n} K_i \mathbf{S}_i \otimes \mathbf{S}_i, \tag{1}$$

in which K_i and $\mathbf{S}_i$ are respectively the nonzero eigenvalues and related hard modes (2nd order symmetric tensor) of $\mathbf{C}$. The material can only sustain stresses in a subspace spanned by $\mathbf{S}_i$. For two-dimensional (2D) cases, bimode (sometimes also called 2D pentamode) and unimode material (UM) are the only two types of extremal materials. The most investigated extremal materials are pentamode materials (PM), because not only are they easy to construct into the simplest elastics, but they also have amazing applications in controlling sound waves [2-12]. On the other hand, auxetic materials, though they are not considered intentionally in context of extremal materials, are familiar examples of UM. For the isotropic case, it is an elastic material with Poisson's ratio approaching -1, and its only soft mode is the dilatation [13-15].

For a d-dimensional ideally pin-jointed truss structure

*Corresponding author. E-mail address: liuxn@bit.edu.cn (Xiaoning Liu)
Executive Editor: Guoliang Huang

with finite size to be stiff, the Maxwell's [16] counting rule $n_b = dn_a - d(d+1)/2$ with n_b and n_a being respectively the number of bars and nodes gives a necessary (yet not sufficient) condition. However, it is a bit different for the case of infinite periodic lattices, for which the average number of bars per node, i.e., the coordination number $Z = 2n_b/n_a$, can be used instead and the Maxwell rule reads in this case $Z = 2d$. Truss structures satisfying $Z = 2d$ are at the verge of mechanical stability and are known as isostatic lattices [17,18]. Recently, there have been great research interests on isostatic lattices since their mechanism modes (floppy modes) can be intentionally localized on the edge with topological protection, representing a static mechanical analog of topological insulators [19,20], which is different from the phononic topology at nonzero-frequencies [21]. Here we distinguish the lattice-level mechanism mode which is nodal displacements producing no bar elongations, and the soft mode which is a macroscopic strain without causing stress and elastic energy. The latter is often referred to as Guest mode for a truss network [22]. Actually, unless in special configuration, isostatic lattices are UM and trimode materials for 2D and 3D, respectively [23]. Because of the single soft mode, UMs possess remarkable features in static and dynamic responses [24-26]. In particular, in view of continuous media and expressing the elasticity problem in complex variables, it is found that the allowable fields of stress-free and stress-bearing displacement in 2D UM are exactly induced by analytic functions [24,25]. On the microstructure side, the concepts were illustrated with known lattices with single mechanism, e.g., Kagome lattice, rotation-square lattice or their distorted versions, and emphasis was placed mainly on the stress-free soft mode.

Although extremal materials have many interesting static and dynamic properties, there are few studies that can give specific configurations for any extremal materials with a prescribed elastic tensor. So far, except for PMs, most works on extremal materials using under-constrained lattices focus on the attainability of soft modes for which case bars can be treated as rigid [1,27]. In that regard, appropriate homogenization method correctly predicting the rank-deficient elastic tensor, which is sensitive in both bar connectivity and stiffness, is not necessary. Recently, truss networks realizing prescribed extremal material elasticity tensor were studied by using topological optimization [28]. Topological optimization methods were usually used to design materials or structures with high stiffness-density ratio [29,30] or singular elasticity [31] rather than with soft modes. In this paper we aim to develop a systematic scheme, including both the homogenization and inverse design, in order to customize both the soft and hard modes of periodic truss lattices. The method is applied and validated in designing 2D extremal materials, but is also illumining for 3D situation.

There have been in-depth studies in literature for the evaluation of effective elastic properties of periodic lattice materials [32-36]. However, for an under-constrained lattice undergoing macroscopic strain, relaxation process due to non-affine local deformations will direct the lattice to a lower energy [37]. In this situation formulations based on the enforcement of affine boundary conditions on a unit cell are no longer appropriate. For truss structures, formulation by matrix and singular value decomposition (SVD) provides an elegant methodology for understanding lattice mechanisms, self-stresses and the load-bearing behavior [38-40]. Together with the aid of Cauchy-Born hypothesis, a homogenization technique capable of settling the non-affine relaxation can be established and is suitable for under-constrained lattice materials [20,41]. The method is adopted in this study to give explicitly the effective elastic tensor in a compact form similar to Eq. (1).

The paper proceeds as follows. In Sect. 2, homogenization based on Cauchy-Born hypothesis and SVD is revisited and compact expression of overall elasticity tensor in hard and soft mode is given for under constrained truss lattices. In Sect. 3, for prescribed rank-deficient elasticity tensor, a two-step design scheme separately seeking the soft and hard mode of extremal materials is suggested, and is applied in 2D case. In Sect. 4, analytic responses in 2D UMs are demonstrated and validated using the designed material. Conclusions are drawn in Sect. 5.

2. Effective elastic tensor of under-constrained truss lattices

The aim of this section is to homogenize a periodic truss network towards a continuum characterized by an elastic tensor $\mathbf{C}$. The equivalence is ensured by equating the macroscopic and microscopic deformation energy density, i.e., $\frac{1}{2}\mathbf{E} : \mathbf{C} : \mathbf{E} = w_{\text{cell}}(\mathbf{E}) / V_{\text{cell}}$ under a macroscopic strain tensor $\mathbf{E}$, where w_{cell} and V_{cell} are the deformation energy and volume of a single unit cell, respectively. Although the homogenization scheme is generally valid for any truss lattice, here it is mainly targeted to under-constrained lattice and rank deficient $\mathbf{C}$. To correctly handle the potentially involved zero energy mode and singularity, the matrix formulation of periodic lattice and SVD based technique will be employed to evaluate the local energy of truss network.

Firstly, consider a d-dimensional truss assembly consisting of n_a nodes (with locations $\mathbf{x}_a$, $a \in [1, 2, \ldots, n_a]$) and n_b bars without external constraints. The tensions and elongations of the n_b bars are assembled into vectors $\mathbf{t}$ and $\mathbf{e}$, and the dn_a displacement and external force components of the nodes are assembled into vectors $\mathbf{u}$ and $\mathbf{f}$, respectively. Balance at each node implies the equilibrium equation in a

matrix form as

$$\mathbf{At} = \mathbf{f}, \tag{2}$$

meanwhile the kinematic equation relating the displacements and bar elongations is

$$\mathbf{Bu} = \mathbf{e}, \tag{3}$$

where the equilibrium matrix $\mathbf{A}$ and kinematic matrix $\mathbf{B}$ are introduced [40]. By using the virtual work principle, $\mathbf{f}^{\mathrm{T}}\delta\mathbf{u} = \mathbf{t}^{\mathrm{T}}\mathbf{A}^{\mathrm{T}}\delta\mathbf{u} = \mathbf{t}^{\mathrm{T}}\delta\mathbf{e} = \mathbf{t}^{\mathrm{T}}\mathbf{B}\delta\mathbf{u}$, it is obvious that $\mathbf{B} = \mathbf{A}^{\mathrm{T}}$, where a superscript T denotes the transpose. Consider for instance bar b linking two nodes a_1 and a_2 with locations $\mathbf{x}_{a_1}$ and $\mathbf{x}_{a_2}$, respectively. A unit vector along the bar is defined as $\hat{\mathbf{r}}_b = (\mathbf{x}_{a_2} - \mathbf{x}_{a_1})/l_b$ with $l_b = \left|\mathbf{x}_{a_2} - \mathbf{x}_{a_1}\right|$ being the bar length. For small deformation the bar elongation is $e_b = (\mathbf{u}_{a_2} - \mathbf{u}_{a_1}) \cdot \hat{\mathbf{r}}_b$, by which it is straightforward to build the $n_{\mathrm{b}} \times dn_{\mathrm{a}}$ matrix $\mathbf{B}$ once the involved variables for nodes and bars are appropriately indexed. Define $\mathbf{h} = \mathrm{diag}[h_1, h_2, \ldots, h_{n_{\mathrm{b}}}]$ with h_b ($b \in [1, 2, \ldots, n_{\mathrm{b}}]$) being the stiffness of bar b and we have $\mathbf{t} = \mathbf{he}$. The mechanical response of the truss under nodal loading can then be solved by

$$\left(\mathbf{AhA}^{\mathrm{T}}\right)\mathbf{u} = \mathbf{Ku} = \mathbf{f}, \tag{4}$$

where $\mathbf{K}$ is the symmetric stiffness matrix with dn_{a} degree of freedoms (DOFs).

Consider an infinitely periodic lattice undergoing a macroscopic strain $\mathbf{E}$, with respect to the Cauchy-Born hypothesis [38], nodal displacements of the lattice can be decomposed into an affine part $\mathbf{u}^{\mathrm{aff}}$ in consistence with the macroscopic strain tensor $\mathbf{E}$, and a cell-wisely periodic part $\mathbf{u}^{\mathrm{p}}$, i.e., $\mathbf{u} = \mathbf{u}^{\mathrm{aff}} + \mathbf{u}^{\mathrm{p}}$, where $\mathbf{u}_a^{\mathrm{aff}} = \mathbf{E} \cdot \mathbf{x}_a$ with $a \in [1, 2, \ldots, n_{\mathrm{a}}]$ is the affine displacement of node a. Accordingly the bar elongation vector also consists of two parts

$$\mathbf{e} = \mathbf{e}^{\mathrm{aff}} + \mathbf{Bu}^{\mathrm{p}}, \tag{5}$$

in which $\mathbf{e}^{\mathrm{aff}} = \left[e_1^{\mathrm{aff}}, e_2^{\mathrm{aff}}, \ldots, e_{n_{\mathrm{b}}}^{\mathrm{aff}}\right]^{\mathrm{T}}$ and the affine elongation of bar $b \in [1, 2, \ldots, n_{\mathrm{b}}]$ is

$$e_b^{\mathrm{aff}} = l_b \hat{\mathbf{r}}_b \cdot \mathbf{E} \cdot \hat{\mathbf{r}}_b. \tag{6}$$

Since $\mathbf{u}^{\mathrm{p}}$ has the same periodicity with the lattice, i.e., for any pair of nodes whose locations differ by a integer multiple of lattice vectors, their nodal displacement components in the vector $\mathbf{u}^{\mathrm{p}}$ take the same value. As a result, $\mathbf{u}^{\mathrm{p}}$ is not independent and one can reduce $\mathbf{u}^{\mathrm{p}}$ into a vector $\tilde{\mathbf{u}}^{\mathrm{p}}$ containing only independent nodal displacement components, and their relation is of the form $\mathbf{u}^{\mathrm{p}} = \mathbf{Q}\tilde{\mathbf{u}}^{\mathrm{p}}$, where $\mathbf{Q}$ is a matrix only contains 0 and 1. The $\mathbf{A}$ and $\mathbf{B}$ matrices correspondingly reduce to $\widetilde{\mathbf{B}} = \widetilde{\mathbf{A}}^{\mathrm{T}} = \mathbf{BQ}$, by which Eq. (5) is rewritten as

$$\mathbf{e} = \mathbf{e}^{\mathrm{aff}} + \widetilde{\mathbf{B}}\tilde{\mathbf{u}}^{\mathrm{p}}. \tag{7}$$

The strain energy density of the lattice is then

$$w = \frac{1}{2V_{\mathrm{cell}}}\left(\mathbf{e}^{\mathrm{aff}} + \widetilde{\mathbf{B}}\tilde{\mathbf{u}}^{\mathrm{p}}\right)^{\mathrm{T}}\mathbf{h}\left(\mathbf{e}^{\mathrm{aff}} + \widetilde{\mathbf{B}}\tilde{\mathbf{u}}^{\mathrm{p}}\right), \tag{8}$$

where V_{cell} is the volume of a unit cell. Given any macro deformation $\mathbf{E}$, $\mathbf{e}^{\mathrm{aff}}$ is determined and the equilibrium state resorts to a solution $\tilde{\mathbf{u}}^{\mathrm{p}}$ which minimizes the stain energy density w. Assuming $\mathrm{rank}(\widetilde{\mathbf{B}}) = n_{\mathrm{r}}$, according to SVD, the matrix can be decomposed into

$$\widetilde{\mathbf{B}} = \widetilde{\mathbf{V}}\widetilde{\mathbf{W}}\widetilde{\mathbf{U}}^{\mathrm{T}}, \tag{9}$$

where $\widetilde{\mathbf{V}} = [\widetilde{\mathbf{V}}_{\mathrm{r}} \;\; \widetilde{\mathbf{V}}_{\mathrm{s}}]$ and $\widetilde{\mathbf{U}} = [\widetilde{\mathbf{U}}_{\mathrm{r}} \;\; \widetilde{\mathbf{U}}_0]$ are orthogonal square matrices of dimensions n_{b} and dn_{a}, respectively, and $\widetilde{\mathbf{W}}$ is a $n_{\mathrm{b}} \times dn_{\mathrm{a}}$ matrix with n_{r} nonzero elements $w_{\gamma\gamma}$ ($\gamma \in [1, 2, \ldots, n_{\mathrm{r}}]$) on the leading diagonal with all other elements being zero. Further, the submatrix:

$$\widetilde{\mathbf{V}}_{\mathrm{s}} = [\mathbf{s}_1\, \mathbf{s}_2\, \ldots\, \mathbf{s}_{n_{\mathrm{s}}}] \tag{10}$$

collects the $n_{\mathrm{s}} = n_{\mathrm{b}} - n_{\mathrm{r}}$ vectors $\mathbf{s}_\alpha$ ($\alpha \in [1, 2, \ldots, n_{\mathrm{s}}]$) representing the self-balanced bar tensions in absence of external nodal loads, named the self-stress state (SSS), spanning the null space of $\widetilde{\mathbf{A}}$. On the other hand, the submatrix

$$\widetilde{\mathbf{U}}_0 = [\mathbf{m}_1\, \mathbf{m}_2 \ldots\, \mathbf{m}_{n_0}] \tag{11}$$

collects the $n_0 = dn_{\mathrm{a}} - n_{\mathrm{r}}$ vectors $\mathbf{m}_\xi$ ($\xi \in [1, 2, \ldots, n_0]$) representing the non-trivial nodal displacements without producing any bar elongation, i.e the mechanism modes of the lattice, spanning the null space of $\widetilde{\mathbf{B}}$, or the left null space of $\widetilde{\mathbf{A}}$. Substituting Eq. (9) into Eq. (8) and noticing the orthogonality of the null spaces and their orthogonal complements, the energy density can be expressed as

$$w = \frac{1}{2V_{\mathrm{cell}}}\begin{bmatrix}\mathbf{e}_{\mathrm{r}}^{\mathrm{aff}} + \widetilde{\mathbf{W}}_{\mathrm{rr}}\tilde{\mathbf{u}}_{\mathrm{r}}^{\mathrm{p}} \\ \mathbf{e}_{\mathrm{s}}^{\mathrm{aff}}\end{bmatrix}^{\mathrm{T}}\begin{bmatrix}\mathbf{h}_{\mathrm{rr}} & \mathbf{h}_{\mathrm{rs}} \\ \mathbf{h}_{\mathrm{sr}} & \mathbf{h}_{\mathrm{ss}}\end{bmatrix}\begin{bmatrix}\mathbf{e}_{\mathrm{r}}^{\mathrm{aff}} + \widetilde{\mathbf{W}}_{\mathrm{rr}}\tilde{\mathbf{u}}_{\mathrm{r}}^{\mathrm{p}} \\ \mathbf{e}_{\mathrm{s}}^{\mathrm{aff}}\end{bmatrix}, \tag{12}$$

where the blocked vectors and matrices with subscripts s and r represent their projections onto the null spaces and its orthogonal complement, respectively, i.e., $\mathbf{e}_{\mathrm{r}}^{\mathrm{aff}} = \widetilde{\mathbf{V}}_{\mathrm{r}}^{\mathrm{T}}\mathbf{e}^{\mathrm{aff}}$, $\mathbf{e}_{\mathrm{s}}^{\mathrm{aff}} = \widetilde{\mathbf{V}}_{\mathrm{s}}^{\mathrm{T}}\mathbf{e}^{\mathrm{aff}}$, $\mathbf{h}_{\mathrm{rs}} = \widetilde{\mathbf{V}}_{\mathrm{r}}^{\mathrm{T}}\mathbf{h}\widetilde{\mathbf{V}}_{\mathrm{s}}$ and $\tilde{\mathbf{u}}_{\mathrm{r}}^{\mathrm{p}} = \widetilde{\mathbf{U}}_{\mathrm{r}}^{\mathrm{T}}\tilde{\mathbf{u}}^{\mathrm{p}}$, etc, and $\widetilde{\mathbf{W}}_{\mathrm{rr}} = \mathrm{diag}[w_{11}, w_{22}, \ldots, w_{n_{\mathrm{r}}n_{\mathrm{r}}}]$. Note that the projection of $\tilde{\mathbf{u}}^{\mathrm{p}}$ on to the null space $\widetilde{\mathbf{U}}_0$ does not contribute and only $\tilde{\mathbf{u}}_{\mathrm{r}}^{\mathrm{p}}$ enters into the energy [20].

To determine the unknown $\tilde{\mathbf{u}}_{\mathrm{r}}^{\mathrm{p}}$, we minimize the energy by

$$\frac{\partial w}{\partial \tilde{\mathbf{u}}_{\mathrm{r}}^{\mathrm{p}}} = \frac{1}{V_{\mathrm{cell}}}\widetilde{\mathbf{W}}_{\mathrm{rr}}^{\mathrm{T}}\begin{bmatrix}\mathbf{h}_{\mathrm{rr}} & \mathbf{h}_{\mathrm{rs}}\end{bmatrix}\begin{bmatrix}\mathbf{e}_{\mathrm{r}}^{\mathrm{aff}} + \widetilde{\mathbf{W}}_{\mathrm{rr}}\tilde{\mathbf{u}}_{\mathrm{r}}^{\mathrm{p}} \\ \mathbf{e}_{\mathrm{s}}^{\mathrm{aff}}\end{bmatrix} = 0, \tag{13}$$

from which it is solved out that

$$\mathbf{e}_{\mathrm{r}}^{\mathrm{aff}} + \widetilde{\mathbf{W}}_{\mathrm{rr}}\tilde{\mathbf{u}}_{\mathrm{r}}^{\mathrm{p}} = -\mathbf{h}_{\mathrm{rr}}^{-1}\mathbf{h}_{\mathrm{rs}}\mathbf{e}_{\mathrm{s}}^{\mathrm{aff}}. \tag{14}$$

Substituting Eq. (14) into Eq. (12), the energy density is expressed solely as the applied affine deformation:

$$w=\frac{1}{2V_{\text{cell}}}\left(\mathbf{e}_{\text{s}}^{\text{aff}}\right)^{\text{T}}\mathbf{h}'_{\text{ss}}\mathbf{e}_{\text{s}}^{\text{aff}}=\frac{1}{2V_{\text{cell}}}\sum_{\alpha=1}^{n_{\text{s}}}\sum_{\beta=1}^{n_{\text{s}}}\left(\mathbf{h}'_{\text{ss}}\right)_{\alpha\beta}\left(\mathbf{e}_{\text{s}}^{\text{aff}}\right)_{\alpha}\left(\mathbf{e}_{\text{s}}^{\text{aff}}\right)_{\beta}, \tag{15}$$

where

$$\begin{aligned}&\mathbf{h}'_{\text{ss}}=\left(\mathbf{h}_{\text{ss}}-\mathbf{h}_{\text{sr}}\mathbf{h}_{\text{rr}}^{-1}\mathbf{h}_{\text{rs}}\right)=\left[\left(\mathbf{h}^{-1}\right)_{\text{ss}}\right]^{-1},\\ &\text{and}\left(\mathbf{h}^{-1}\right)_{\text{ss}}=\widetilde{\mathbf{V}}_{\text{s}}^{\text{T}}\left(\mathbf{h}^{-1}\right)\widetilde{\mathbf{V}}_{\text{s}}.\end{aligned} \tag{16}$$

The projection of affine bar elongations onto each SSS state vector $\mathbf{s}_\alpha$ is evaluated by using Eq. (6) as

$$\left(\mathbf{e}_{\text{s}}^{\text{aff}}\right)_{\alpha}=\sum_{b=1}^{n_{\text{b}}}e_b^{\text{aff}}s_{\alpha b}=\sum_{b=1}^{n_{\text{b}}}\left(l_b\hat{\mathbf{r}}_b\cdot\mathbf{E}\cdot\hat{\mathbf{r}}_b\right)s_{\alpha b}=\mathbf{E}:\bar{\mathbf{S}}_\alpha, \tag{17}$$

where $s_{\alpha b}$ is the bth element of the self-stress vector $\mathbf{s}_\alpha$, and a symmetric tensor with order two is defined for each SSS mode:

$$\bar{\mathbf{S}}_\alpha=\sum_{b=1}^{n_{\text{b}}}\left(\hat{\mathbf{r}}_b\otimes\hat{\mathbf{r}}_b\right)s_{\alpha b}l_b. \tag{18}$$

Finally, the strain energy density of a periodic truss lattice undergoing an applied macroscopic strain $\mathbf{E}$ can be compactly expressed as

$$w=\frac{1}{2}\mathbf{E}:\mathbf{C}:\mathbf{E}, \tag{19}$$

where

$$\mathbf{C}=\frac{1}{V_{\text{cell}}}\sum_{\alpha=1}^{n_{\text{s}}}\sum_{\beta=1}^{n_{\text{s}}}\left[\left(\mathbf{h}'_{\text{ss}}\right)_{\alpha\beta}\bar{\mathbf{S}}_\alpha\otimes\bar{\mathbf{S}}_\beta\right] \tag{20}$$

can be obviously regarded as the homogenized elastic tensor. If the bars possess uniform stiffness constant h, then $\left(\mathbf{h}'_{\text{ss}}\right)_{\alpha\beta}=h\delta_{\alpha\beta}$, the effective elastic tensor can be simplified as

$$\mathbf{C}=\frac{h}{V_{\text{cell}}}\sum_{\alpha=1}^{n_{\text{s}}}\bar{\mathbf{S}}_\alpha\otimes\bar{\mathbf{S}}_\alpha. \tag{21}$$

The homogenization is valid for both 2D and 3D truss lattices regardless the effective elastic tensor is of full rank or not.

3. Microstructural design

3.1 Two-step design scheme

The homogenization process actually tells us how soft and hard modes are generated at the microscopic level. When any uniform macroscopic deformation $\mathbf{E}$ occurs on an under-constrained lattice, it may undergo a periodic and non-affine deformation field $\tilde{\mathbf{u}}^{\text{p}}$ to reduce the energy. According to the truss connectivity, full vector space of possible bar elongation $\mathbf{e}$ is isolated into two subspaces orthogonal to each other, namely the column space of kinematic matrix, col($\widetilde{\mathbf{B}}$), and the kernel space of its transpose, ker$\left(\widetilde{\mathbf{B}}^{\text{T}}\right)$. As shown in Eq. (7), only the projection of $\mathbf{e}^{\text{aff}}$ on col($\widetilde{\mathbf{B}}$) could be released by $\tilde{\mathbf{u}}^{\text{p}}$. In certain cases, the affine elongation vector $\mathbf{e}^{\text{aff}}$ due to the deformation $\mathbf{E}=\mathbf{E}_0$ lies completely in col($\widetilde{\mathbf{B}}$). As a result, $\mathbf{e}^{\text{aff}}$ can be totally relaxed such that

$$\widetilde{\mathbf{B}}\tilde{\mathbf{u}}^{\text{p}}+\mathbf{e}^{\text{aff}}=\mathbf{e}=\mathbf{0}, \tag{22}$$

which means $\mathbf{E}_0$ is a soft mode. Conversely, the projection of $\mathbf{e}^{\text{aff}}$ on ker$\left(\widetilde{\mathbf{B}}^{\text{T}}\right)$ contributes deformation energy resisting a macroscopic deformation. In conclusion, it's SSSs of the lattice that generate the space of hard modes. Note that, however, not every SSS at the micro level will result in a hard mode. Only the intersection of ker$\left(\widetilde{\mathbf{B}}^{\text{T}}\right)$ and the subspace of the elongation vector of which any element definitely results from a certain affine deformation, contributes to the hard mode in macroscopic level. Therefore, the necessary condition for the full rank of the effective elastic tensor of a lattice is dim ker$\left(\widetilde{\mathbf{B}}^{\text{T}}\right)\geq d(d+1)/2$.

The relationship between the above-mentioned orthogonal spaces at the macro and micro levels is concluded in Fig. 1. For a rank deficient elastic tensor $\mathbf{C}$, an eigenvalue analysis isolates the spaces of soft and hard modes with basis $\mathbf{E}_{0j}$ and $\mathbf{S}_i$, respectively. The $\mathbf{E}_{0j}$ space maps to the affine bar elongations $\mathbf{e}^{\text{aff}}$ which lie in column space of the reduced kinematic matrix col($\widetilde{\mathbf{B}}$), and basis of null-space of the equilibrium matrix ker$\left(\widetilde{\mathbf{B}}^{\text{T}}\right)$ contribute in turn to the hard modes of an extremal material. Note that the $\widetilde{\mathbf{B}}$ matrix depends only on geometry information of the lattice, so do the spaces of soft mode and hard modes. However, the components and magnitudes of an elastic tensor are determined by the bar stiffness parameters.

Given an arbitrary rank-deficient $\mathbf{C}$, the inverse process for finding the lattice usually resorts to an optimization algorithm. Based on the previous discussion, a two-step design scheme is proposed: (1) choose a lattice linking topology (with the help of the counting rule) and search the lattice geometry leading exactly to col($\widetilde{\mathbf{B}}$), at the same time SSSs of the lattice are also prepared; (2) search the bar stiffness parameters mixing the self-stress modes to produce

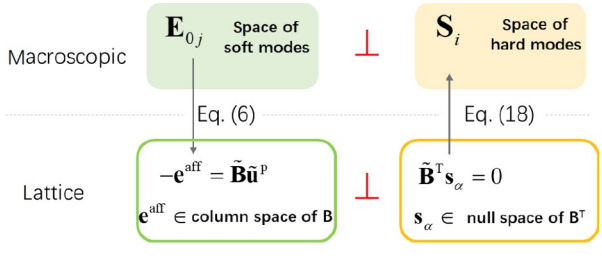

Figure 1 Orthogonal spaces on macroscopic and lattice level.

the required rank-deficient elastic tensor. The optimization process is detailed by the flowchart shown in Fig. 2. For any prescribed elastic tensor of an extremal material, firstly, its target hard modes and soft modes can be isolated by the eigenvalue decomposition of the elastic tensor. According to the two-step scheme introduced above, the geometric parameters, such as positions of joints in a cell, are optimized to let the lattice possess and only possess the target soft modes. The indicator δ in Fig. 2 is used to monitor this discrepancy. If the first step is finished, the isolation of the subspaces of hard modes and soft modes is achieved. The second procedure then runs over the bar stiffnesses to drive the effective elastic tensor approaching to the target one. Though the suggested design scheme is generally suggested for any extremal material, here in the following it is applied in 2D case and mainly focuses on 2D UMs.

3.2 Direct construction of 2D UM by superposing two PM lattices

Before calling in material design with optimization algorithm, we first consider building UM by directly superposing two PM lattices. The honeycomb topology shown in Fig. 3a is the simplest lattice topology for designing PMs, first proposed by Milton and Cherkaev [1].

Let the origin, $\mathbf{a}_1$, $\mathbf{a}_2$, and $\mathbf{p}$ be respectively the locations of nodes 1-4 with $\mathbf{a}_1 = (a, -b)$, $\mathbf{a}_2 = (a, b)$ being the lattice vectors. The bar vectors are $\hat{\mathbf{r}}_1 = -\mathbf{p}/l_1$, $\hat{\mathbf{r}}_2 = (\mathbf{a}_1 - \mathbf{p})/l_2$, $\hat{\mathbf{r}}_3 = (\mathbf{a}_2 - \mathbf{p})/l_3$ with $l_1 = |\mathbf{p}|$, $l_2 = |\mathbf{a}_1 - \mathbf{p}|$, $l_3 = |\mathbf{a}_2 - \mathbf{p}|$. The node displacement vector is $\mathbf{u}^{\mathrm{p}} = \left(\mathbf{u}_1^{\mathrm{T}} \quad \mathbf{u}_2^{\mathrm{T}} \quad \mathbf{u}_3^{\mathrm{T}} \quad \mathbf{u}_4^{\mathrm{T}}\right)^{\mathrm{T}}$ and the kinematic matrix is

$$\mathbf{B} = \begin{bmatrix} -\hat{\mathbf{r}}_1^{\mathrm{T}} & \mathbf{0} & \mathbf{0} & \hat{\mathbf{r}}_1^{\mathrm{T}} \\ \mathbf{0} & -\hat{\mathbf{r}}_2^{\mathrm{T}} & \mathbf{0} & \hat{\mathbf{r}}_2^{\mathrm{T}} \\ \mathbf{0} & \mathbf{0} & -\hat{\mathbf{r}}_3^{\mathrm{T}} & \hat{\mathbf{r}}_3^{\mathrm{T}} \end{bmatrix}. \tag{23}$$

Considering the periodic condition of $\mathbf{u}^{\mathrm{p}}$, there are only two independent nodes in a cell. Here we choose

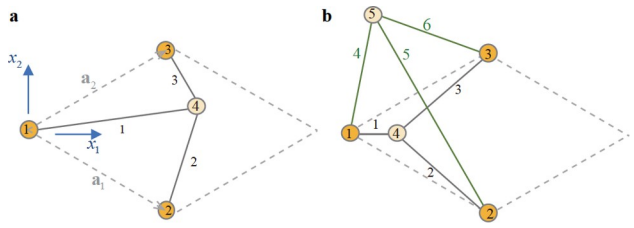

Figure 3 **a** Unit cell of PM consists three bars and the coordination number $Z = 3$. **b** Unit cell of UM by superposing two PMs, $Z = 4$.

$\tilde{\mathbf{u}}^{\mathrm{p}} = \left(\mathbf{u}_1^{\mathrm{T}} \quad \mathbf{u}_4^{\mathrm{T}}\right)^{\mathrm{T}}$, and the matrix $\mathbf{Q}$ can be obtained as

$$\mathbf{Q} = \begin{bmatrix} \mathbf{I} & \mathbf{0} \\ \mathbf{I} & \mathbf{0} \\ \mathbf{I} & \mathbf{0} \\ \mathbf{0} & \mathbf{I} \end{bmatrix}, \tag{24}$$

such that $\mathbf{u}^{\mathrm{p}} = \mathbf{Q}\tilde{\mathbf{u}}^{\mathrm{p}}$ and $\mathbf{I}$ is the 2×2 identity matrix. The reduced kinematic matrix and the equilibrium matrix are respectively,

$$\tilde{\mathbf{B}} = \begin{bmatrix} -\hat{\mathbf{r}}_1^{\mathrm{T}} & \hat{\mathbf{r}}_1^{\mathrm{T}} \\ -\hat{\mathbf{r}}_2^{\mathrm{T}} & \hat{\mathbf{r}}_2^{\mathrm{T}} \\ -\hat{\mathbf{r}}_3^{\mathrm{T}} & \hat{\mathbf{r}}_3^{\mathrm{T}} \end{bmatrix} \text{ and } \tilde{\mathbf{A}} = \begin{bmatrix} -\hat{\mathbf{r}}_1 & -\hat{\mathbf{r}}_2 & -\hat{\mathbf{r}}_3 \\ \hat{\mathbf{r}}_1 & \hat{\mathbf{r}}_2 & \hat{\mathbf{r}}_3 \end{bmatrix}. \tag{25}$$

The self-stress (s_1, s_2, s_3) should set the nodes 4 and 1 in the force balance state, i.e., $s_1\hat{\mathbf{r}}_1 + s_2\hat{\mathbf{r}}_2 + s_3\hat{\mathbf{r}}_3 = 0$, which gives

$$\frac{s_2}{l_2}\mathbf{a}_1 + \frac{s_3}{l_3}\mathbf{a}_2 = \left(\frac{s_1}{l_1} + \frac{s_2}{l_2} + \frac{s_3}{l_3}\right)\mathbf{p}. \tag{26}$$

Equation (26) together with the normalization condition $s_1^2 + s_2^2 + s_3^2 = 1$ can be used to solve the self-stress. Referring to Eq. (18), the only hard mode can be expressed as

$$\begin{aligned} \bar{\mathbf{S}} &= \sum_{b=1}^{3} \hat{\mathbf{r}}_b \otimes \hat{\mathbf{r}}_b \, s_b l_b \\ &= \mathbf{a}_1 \otimes \mathbf{a}_1 \frac{s_2}{l_2} + \mathbf{a}_2 \otimes \mathbf{a}_2 \frac{s_3}{l_3} - \mathbf{p} \otimes \mathbf{p}\left(\frac{s_1}{l_1} + \frac{s_2}{l_2} + \frac{s_3}{l_3}\right). \end{aligned} \tag{27}$$

It can be concluded from Eq. (27) that the hard mode, or

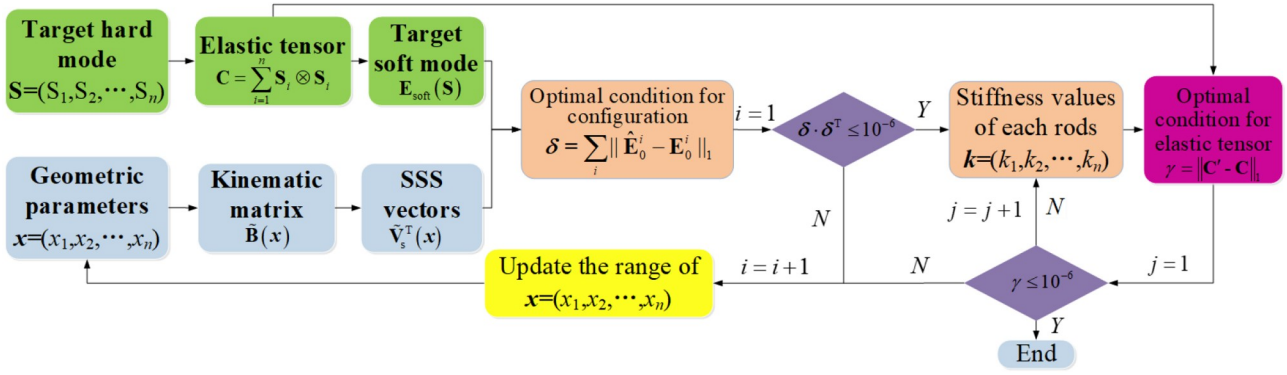

Figure 2 Flow chart for designing extremal materials with any prescribed elastic tensors.

equivalently the two orthogonal soft modes, are determined if the position of node 4 and basis vectors are specified. In design of an individual PM, boundary nodes 1-3 could be fixed and let node 4 move. For a given $\mathbf{S} = \sqrt{h/V_{\text{cell}}}\,\bar{\mathbf{S}}$ with h being the uniform bar stiffness, the coordinates $\mathbf{p} = (x, y)$ of node 4 can be at first solved out by Eqs. (26) and (27) requiring that $\bar{\mathbf{S}}$ is parallel to $\mathbf{S}$. Next, the bar stiffness h is obtained by the ratio factor of $\mathbf{S}$ to $\bar{\mathbf{S}}$.

An UM of elastic tensor $\mathbf{C} = \mathbf{S}_1\otimes\mathbf{S}_1 + \mathbf{S}_2\otimes\mathbf{S}_2$ can be constructed by superposition of two PMs, and each PM is responsible for one characteristic stress $\mathbf{S}_i$. As shown in Fig. 3b, one copy of PM consists of bars (1, 2, 3) with the same stiffness h_1, and the other consists of bars (4, 5, 6) with h_2, illustrating with different colors. It is also required that bars from each PM stand on the same lattice sites, i.e., in the unit cell shown by the dashed parallelogram, both PMs have nodes (1, 2, 3) on the lattice sites as their boundary nodes, and nodes 4 and 5 are internal. Only in doing so, the two SSSs of the six bars under periodic boundary condition take the form $\mathbf{s}_1 = [s_1, s_2, s_3, 0, 0, 0]$, $\mathbf{s}_2 = [0, 0, 0, s_4, s_5, s_6]$, therefore $\mathbf{h}'_{\text{ss}}$ is diagonal and Eq. (21) is just the simple sum of $\mathbf{S}\otimes\mathbf{S}$ of individual PMs.

A design example can be given for verification. Adopting a triangular lattice $a = \sqrt{3}$, $b = 1$ with the unit cell area $V_{\text{cell}} = 2\sqrt{3}$. Two hard modes are arbitrarily chosen as

$$\mathbf{S}_1 = \begin{bmatrix} 2 & 0 \\ 0 & 1 \end{bmatrix}, \quad \mathbf{S}_2 = \begin{bmatrix} 0.250 & 1.299 \\ 1.299 & -1.250 \end{bmatrix}, \tag{28}$$

and the corresponding elasticity matrix in Voigt format reads

$$[\mathbf{C}] = \begin{pmatrix} 4.0625 & 1.6875 & 0.4593 \\ 1.6875 & 2.5625 & -2.2964 \\ 0.4593 & -2.2964 & 3.3750 \end{pmatrix}. \tag{29}$$

It follows that the soft mode of this UM satisfying $\mathbf{E}_0 : \mathbf{S}_1 = \mathbf{E}_0 : \mathbf{S}_2 = 0$ is

$$\mathbf{E}_0 = \begin{pmatrix} 0.3716 & -0.3934 \\ -0.3934 & -0.7433 \end{pmatrix}. \tag{30}$$

By using the mentioned procedure above, individual PMs with $\bar{\mathbf{S}}$ proportional respectively to $\mathbf{S}_1$ and $\mathbf{S}_2$ are found with the internal nodes 4 and 5 located at (0.57735, 0) and (0.28869, 1.50003), respectively, and the bar stiffnesses are uniformly $h = 8.66$ for the six bars and the unit cell configuration is shown in Fig. 3b.

The design of UM by superposing two PMs is robust and theoretically can achieve any pair of characteristic stresses $\mathbf{S}_i$. The method starts from the hard mode space and provides an explicitly one-to-one correspondence to $\mathbf{S}_i$. However, the drawback is also obvious since bar intersections are unavoidable, thus it is infeasible for practical purposes. A more complex lattice topology without bar intersection is presented in the following.

3.3 Optimization UM design based on eight-bar configuration

According to Maxwell-Calladine counting rule [20,40], lattices with $Z = 4$ satisfy the relation in the periodic condition, $dn_a - n_b = n_0 - n_s = 0$, which means that the number of the SSSs and ZMs are equal. In the periodic condition, there must be at least two ZMs, rigid translation along x and y directions, so does the number of SSS. Therefore, in most cases the lattices with $Z = 4$ are potential candidates for the UM design. In another perspective, the cell for UMs must be a single DOF system that supports the only mechanism for the soft mode of the UM. The lattice connectivity and numbering are shown in Fig. 4 by a unit cell containing eight bars and six nodes, four of which are independent. The cells are also arranged in a triangular lattice by lattice vectors $\mathbf{a}_1 = (a, -b)$, $\mathbf{a}_2 = (a, b)$.

Assuming the cell geometry is symmetric with respect to the x-axis, obviously its soft mode is of the form $\mathbf{E}_0 = \text{diag}(\varepsilon_x, \varepsilon_y)$ in the coordinate system shown in the figure, and can be checked out manually by examining the mechanism. Excluding nodes 1 (a, 0) and 2 (0, b) on the Bravais lattice sites, the locations of nodes 3 and 4 can be used to tune the soft mode. For convenience, we use the length l_8 of bar 8 and an angle β, as shown in Fig. 4, to parametrize location of node 4, thus we totally have three designing parameters (x_3, β, l_8) with x_3 denoting the position of node 3 on the x-axis. The soft mode can be determined as follows. Supposing we fix node 3 and let node 1 move on x-axis to remove the rigid body modes, based on lattice site displacements $\mathbf{u}_1 = (u_{1x}, 0)$ and $\mathbf{u}_2 = (u_{2x}, u_{2y})$, as indicated by red arrows in Fig. 4, the soft strain can be easily determined as $\varepsilon_x = (u_{1x} - u_{2x})/a$ and $\varepsilon_y = u_{2y}/b$, and it is sufficient to use their ratio $\varepsilon_y/\varepsilon_x$. It is straightforward to solve the relation of $\mathbf{u}_1$ and $\mathbf{u}_2$ from the kinematics of the lattice as $u_{2x} = bu_{1x}/[(a - x_3)\tan\beta]$, $u_{2y} = x_3 u_{1x}/[(a - x_3)\tan\beta]$, with which the soft mode is related to the design parameters as

$$\frac{\varepsilon_y}{\varepsilon_x} = \frac{x_3 a/b}{(a - x_3)\tan\beta - b}. \tag{31}$$

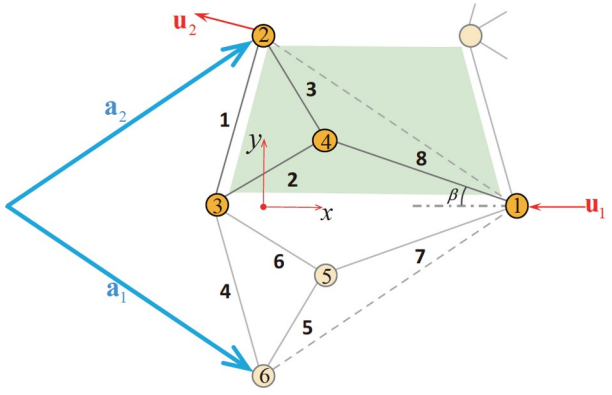

Figure 4 Unit cell of UM containing eight bars without bar intersection.

Note that only the angle β matters and l_8 is irrelevant. As an example, we fix $a = \sqrt{3}$, $b = 1$ and $x_3 = -0.3$ and plot available $\varepsilon_y/\varepsilon_x$ in Fig. 5a as node 4 traverses the unit cell. To avoid bar intersection in the cell tessellation, the movement of node 4 is confined in the shaded light green region shown in Fig. 4 according to the position of node 3. It is seen from the figure that very wide $\varepsilon_y/\varepsilon_x$ ratio including both auxetic and non-auxetic mode can be reached (for better coloring the legend is truncated to $[-5, 5]$ and values exceeding this range are shown in white). For fixed x_3 all points on a line by angle β have the same ratio value and thus the same soft mode, selection of them should be based on the reasonable geometry and achievable hard modes. Lines of $\varepsilon_y/\varepsilon_x = 1$ and -2 are indicated in the figure, and the unit cell geometries corresponding to four points labelled by A-D on the lines are displayed in the insets below. Figure 5b shows the similar plot for $x_3 = 0.3$, it is seen that the auxetic and non-auxetic regions are switched and the attainable $\varepsilon_y/\varepsilon_x$ ratio range is slightly different.

Based on this lattice topology, we still choose to design the UM with the elastic tensor in Eq. (29). The target soft mode in this principal system is by diagonalizing Eq. (30) as $\mathbf{E}_0 = \mathrm{diag}(-0.8661, 0.4964)$, thereby the ratio $\varepsilon_y/\varepsilon_x = -0.5719$ and is highlighted in Fig. 5a by the pink dashed line, on which we choose a location ($x_4 = 0.9$, $y_4 = 0.7815$, marked by the circle) for node 4. With this geometry, $\mathbf{E}_0$ is ensured and the other two hard modes will determinatively orthogonal to $\mathbf{E}_0$ whatever the bar stiffnesses are, we are then left to optimize the eight bar stiffnesses to match the exact values of $\mathbf{C}$.

The optimization is done by Mathematica software using the differential evolution algorithm to minimize the error defined by $\|\mathbf{C}' - \mathbf{C}\|_1$ in which $\mathbf{C}'$ is iteratively calculated by the homogenization method in Sect. 2. Note that the target $\mathbf{C}$ in Eq. (29) should be transformed to the unit cell's principle system, which is in this case rotated anticlockwise by $\phi = 72.4°$. Design space of the bar stiffness is limited in the range $h_i = [1.0, 30.0]$. The optimized nodal locations and bar stiffnesses are listed in the first row of Table 1 with the convergence error 10^{-8}. The final lattice configuration is presented in Fig. 6a by 2×2 unit cells in which bar thicknesses reflect relative values of the square root of stiffnesses. Therein, the principal system is rotated by ϕ with respect to the global, within which the elastic matrix perfectly agrees with Eq. (29).

As an alternative route, we demonstrate here in Fig. 6b another version of design implementing the same elastic matrix. In this version the symmetry of the cell geometry as in Fig. 4 is discarded, and the positions of nodes 3, 4 and 5 are free to tune the lattice, therefore there are totally 14

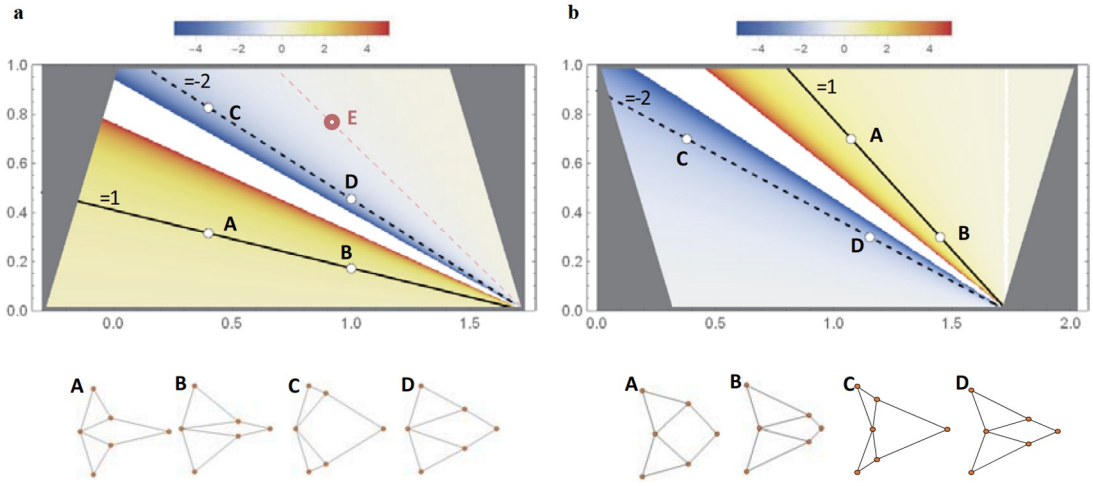

Figure 5 Contour plots for attainable $\varepsilon_y/\varepsilon_x$ ratios of the soft mode for fixed **a** $x_3 = -0.3$ and **b** $x_3 = 0.3$ as node 4 traverses in the unit cell. Insets below selectively demonstrate the cell geometries.

Table 1 Geometry and stiffness details of the designed extremal materials

Symmetric UM in Fig. 6a	h_1 8.5665	h_2 29.998	h_3 9.7785	h_4 14.309	h_5 14.166	h_6 9.3147	h_7 8.3246	h_8 5.1723
	$(x,y)_{1\text{-}6}$ = (1.7321, 0) (0, 1) (−0.3, 0) (0.9, 0.7815) (0.9, −0.7815) (0, −1)							
Asymmetric UM in Fig. 6b	17.887	12.889	2.9358	7.5852	25.662	4.1176	49.999	33.406
	$(x,y)_{1\text{-}6}$ = (0, 0) (1.1454, 0.4210) (1.7810, 1.2365) (1.1410, 0.7413) (2, 0) (1, 1.5)							
Asymmetric PM in Fig. 6c	35.75	2.111	20.497	36.266	50	–	13.752	50
	$(x,y)_{1\text{-}6}$ = (0, 0) (1.1266, 0.2911) (1.674, 0.8726) (1.0, 0.38) (2, 0) (1, 1.5)							
Asymmetric PM in Fig. 6d	8.476	18.630	22.297	12.840	50	–	39.780	19.722
	$(x,y)_{1\text{-}6}$ = (0, 0) (1.7, −0.2) (1.8, 0.8544) (1.0, 0.2225) (2, 0) (1, 1.5)							

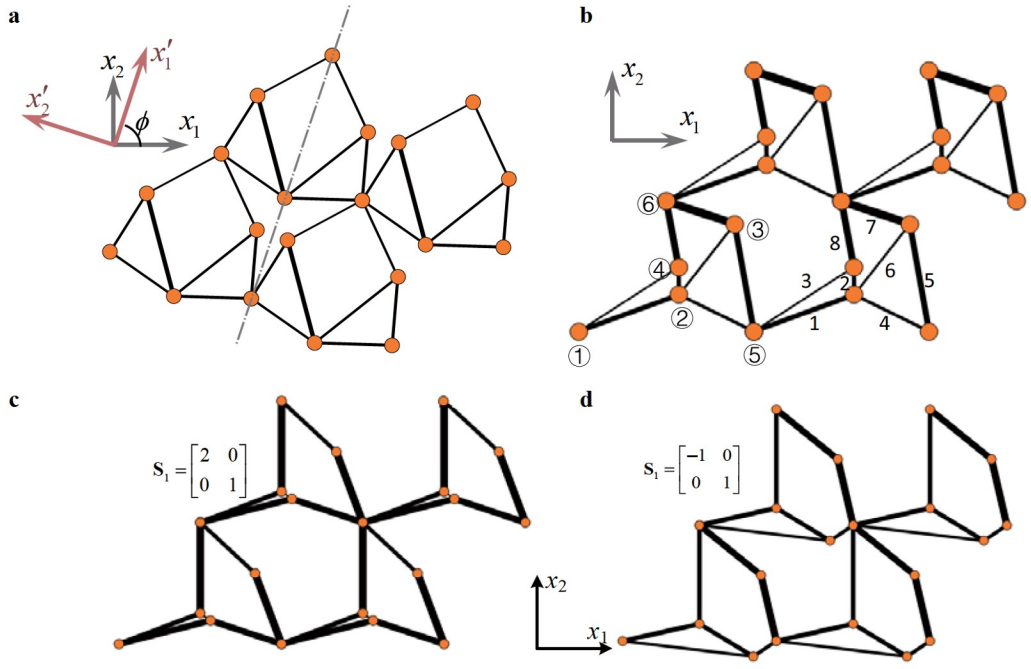

Figure 6 Designed UMs using **a** symmetric and **b** asymmetric configurations on demand of the same effective elastic tensor, Eq. (29) and the designed PMs **c** and **d** for different characteristic stresses. Bar thickness represents the relative value of bar stiffness square root.

design variables including the bar stiffnesses. In this situation it is not possible to figure out the lattice geometry for the soft mode manually. A two-step scheme is still used separately for the soft and hard mode spaces. Locations of nodes 3, 4 and 5 are first searched by optimization to match the soft mode according to Eq. (22), with their relative locations carefully ruled to avoid bar intersection. In this step the optimization is found pretty sensitive to the initial values of design variables and is easy to drop in local minimal. In contrast, once the soft mode is fixed the second step searching the hard modes is always quite stable. The obtained nodal locations and bar stiffnesses are listed in the second row of Table 1. It is seen from the table and Fig. 6b that the bar stiffnesses are quite dispersed compared to the previous design. Though the three UMs in this and the previous subsection all satisfy the prescribed elastic tensor, the one in Fig. 6a is more preferable from the practical viewpoint since its relatively regular shape and uniform bar stiffnesses.

Besides UMs, the variant of the lattice topology in Fig. 4 could also be used for PMs by removing one bar to add a ZM supporting one more soft mode. We test the lattices topology similar to that for UMs, but with bar 6 deleted, which indeed behaves as PMs. Figure 6c and d exhibits two final cell configurations respectively satisfying the characteristic stresses $\mathbf{S} = [2, 0; 0, 1]$ and $[-1, 0; 0, 1]$. The node positions and bar stiffnesses are shown in last two columns of Table 1.

Finally, it should be remarked that it is currently difficult to prove theoretically whether the 8-bar model for UMs or the 7-bar model for PMs are sufficient, or how complex the unit cell should be, to achieve an arbitrary extremal material elastic tensor. In case of more targeted applications, or in consideration of practicability, material design with lattice models of other lattice topologies can also be examined, but the two-step strategy and the optimization process are the same.

4. Mechanical fields in aggregated UM cells

For a piece of material made of fine tessellation of UM cells, obviously a linear displacement field corresponding to rigid body motion or uniform soft strain produces no strain energy. However, in view of 2D UM continuum, it is possible that a quite complex nonlinear displacement field can be free of strain energy too, which is distinct to classical materials. Recently, it was revealed that expressing the elasticity problem in complex variables, such displacement fields fall exactly in complex analytic functions [24,25]. Meanwhile, a duality also holds in that the equilibrium stress field free of body forces resides also in the same family of analytic functions. These findings profoundly decompose a general displacement field in UM into zero-energy and stress-bearing parts. Further, the salient feature of analytic function makes it easier to probe the functionality of UM *a priori*, without resorting to the solution of a complete boundary value problem. With the proposed design technique of both soft and hard mode of UM, we are able to explore and materialize such analysis more purposefully.

Here, the concept of analytic stress-free and stress-bearing

displacement field is illustrated with the designed material example in the previous section. Taking the unimode elasticity tensor of Eq. (29) and functions of cubic polynomial as an example, it can be shown that for a piece of continuous medium the following displacement field will generate no stress in the material:

$$\begin{aligned} u_x^0 &= -0.1295x^2 - 0.8161xy + 0.6049y^2 - 0.5232x^3 \\ &\quad -0.3170x^2y - 2.468xy^2 + 1.530y^3, \\ u_y^0 &= 0.6822x^2 + 0.5179xy + 0.8161y^2 + 1.213x^3 \\ &\quad +3.139x^2y + 0.6340xy^2 + 1.645y^3. \end{aligned} \tag{32}$$

In sharp comparison, a cubic stress-bearing displacement field supported by the medium is

$$\begin{aligned} u_x^s &= -0.2611x^2 - 0.5526xy + 0.5221y^2 - 0.8452x^3 \\ &\quad -2.879x^2y + 0.6167xy^2 + 2.180y^3, \\ u_x^s &= -0.6076x^2 + 1.286xy + 1.215y^2 - 0.6994x^3 \\ &\quad -0.2097x^2y + 4.977xy^2 + 3.381y^3. \end{aligned} \tag{33}$$

In the derivation of Eqs. (32) and (33), in which the soft mode (Eq. (30)) and hard modes (Eq. (28)) have been encoded, the details can be found in Appendix and in Ref. [25].

These two types of cubic displacement field are enforced to a finite lattice consisting of 16 × 16 designed unit cells as shown in Fig. 6b, the resulting deformation and bar tensions are shown in Fig. 7. It is seen that although the deformations for the two cases are both significant, in Fig. 7a almost zero bar tensions and nodal reactions are observed for the stress-free displacement. Conversely, in Fig. 7b the stress-bearing displacement field induces obvious bar tensions, thus reaction forces indicated by black arrows are also found on the domain boundary. It is remarkable that the reaction forces exist only on the nodes at cutting edge and remain zero for internal nodes, since this stress-bearing displacement field corresponds to equilibrated stress field of zero body force, $\nabla \cdot \boldsymbol{\sigma} = 0$. Besides, upon the application of the stress-bearing displacement field, it can be verified that the macroscopic stress field $\boldsymbol{\sigma} = V_{\text{cell}}^{-1} \sum_b^{n_b} t_b l_b \left(\hat{\mathbf{r}}_b \otimes \hat{\mathbf{r}}_b \right)$ extracted from the lattice completely lies in the space of hard modes of the designed material, i.e., $\boldsymbol{\sigma}(x,y) = \sigma_1(x,y)\mathbf{S}_1 + \sigma_2(x,y)\mathbf{S}_2$. Fields of σ_1 and σ_2 corresponding to the stress-bearing displacement are contoured in Fig. 7c, where the theoretical one and those extracted from the lattice are compared. As the lattice becomes finer it is seen that the integrated stress field $\sqrt{\sigma_1^2 + \sigma_2^2}$ converges to the theoretical result for both types of the enforced displacement field.

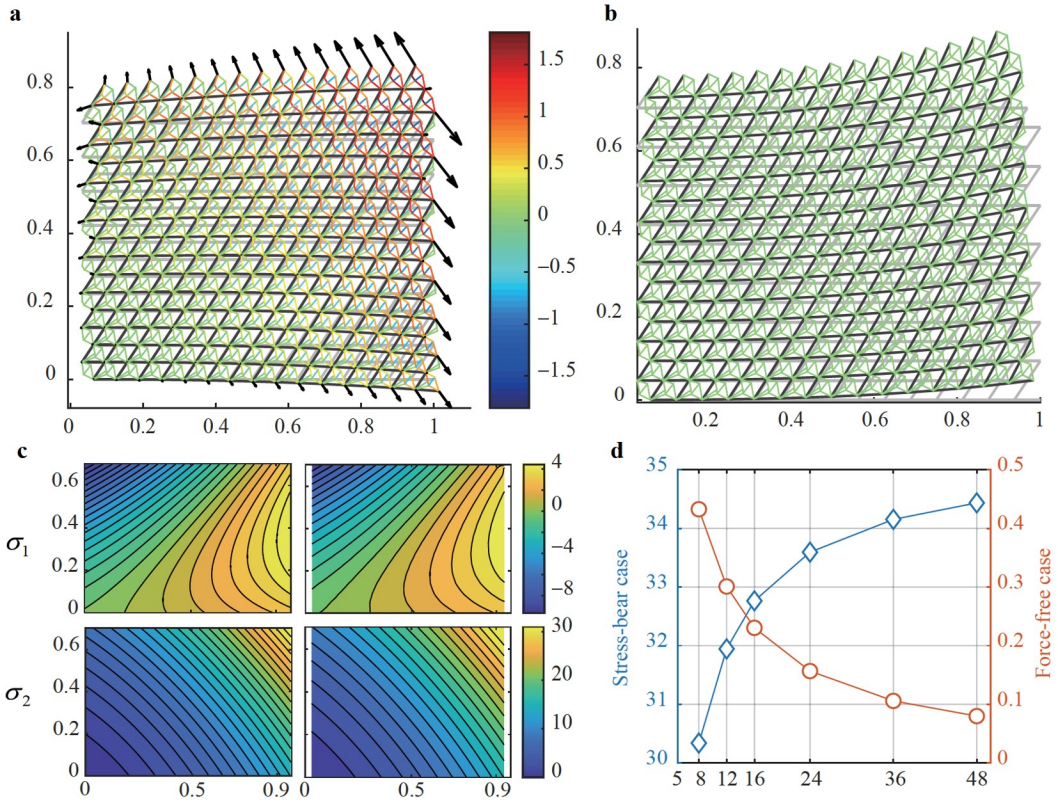

Figure 7 Responses of a finite lattice with the designed microstructure under cubic displacement fields which respectively causes **a** nonzero and **b** zero bar tension. The lattice size is 16 × 16, and cell deformation is highlighted in black lines compared with the undeformed one in gray. Arrows show the nodal reaction forces. The extracted stress fields of σ_1 and σ_2 are shown in the right two contour plots of **c** compared with the analytical fields on the left. **d** Convergence of extracted stresses as function of cell density.

5. Conclusion and discussion

In this work, we have conducted a comprehensive study aiming to extend the design of extremal materials from the well-studied PMs to more general classes. Quite different with the previous efforts on under-constrained lattices, the matching of both soft and hard modes is emphasized in the design process. As a result, following the proposed design scheme in this paper, a concrete truss lattice can be found corresponding to any specific elastic tensor of 2D extremal materials. Though the developed method is testified only in 2D cases, some versatile points of this work including the homogenization technique, the scheme of separate searching in soft and hard mode spaces, the counting consideration on the cell topology as well as the skills in determining the lattice geometry, are enlightening for the design of other extremal lattice materials. With the help of this method, many interesting static and dynamic properties of extremal materials can be materialized by concrete microstructures. This paves the way for the practical utilization of extremal materials. Future applications of under-constrained materials and structures include soft robots, stents, space deployable structures and other shape-morphing structures, whatever the purpose, microstructural kinematics design, as done in this and other works [42-44], is an essential step in order.

Appendix: Analytic stress-free and stress-bearing fields

As revealed in Ref. [25], the analytic essence of the elastic field of 2D continuous UM is formulated in the principal coordinate system in which the soft strain $\mathbf{E}_0$ is diagonalized, e.g., the $x'-y'$ system shown in Fig. 6 for the designed example. In this coordinate system, a set of canonical bases for the soft and hard modes can be chosen as

$$\mathbf{e}_0 = A\begin{bmatrix} 1 & 0 \\ 0 & -\nu \end{bmatrix},\ \mathbf{e}_1 = A\begin{bmatrix} \nu & 0 \\ 0 & 1 \end{bmatrix},\ \mathbf{e}_2 = \begin{bmatrix} 0 & 1 \\ 1 & 0 \end{bmatrix}, \tag{A1}$$

where $A = \sqrt{2/\left(1+\nu^2\right)}$ and ν is the Poisson's ratio in the principal system. With changing of basis, i.e., $\boldsymbol{\sigma} = \sigma_0\mathbf{e}_0 + \sigma_1\mathbf{e}_1 + \sigma_2\mathbf{e}_2$ and $\boldsymbol{\varepsilon} = \varepsilon_0\mathbf{e}_0 + \varepsilon_1\mathbf{e}_1 + \varepsilon_2\mathbf{e}_2$ the elasticity matrix of any UM possesses the following form:

$$\begin{pmatrix} \sigma_0 \\ \sigma_1 \\ \sigma_2 \end{pmatrix} = \begin{bmatrix} 0 & 0 & 0 \\ 0 & C_{11} & C_{12} \\ 0 & C_{12} & C_{22} \end{bmatrix}\begin{pmatrix} \varepsilon_0 \\ \varepsilon_1 \\ \varepsilon_2 \end{pmatrix}.$$

For the designed example (Eqs. (28)-(30)), it follows that $\nu = 0.5719$, $C_{11} = 5.3709$, $C_{12} = 0.6519$, $C_{22} = 4.6291$. The following transformation of coordinate and field variables:

$$\begin{pmatrix} w \\ \overline{w} \end{pmatrix} = \begin{bmatrix} 1 & 1/\gamma \\ 1 & -1/\gamma \end{bmatrix}\begin{pmatrix} x' \\ y' \end{pmatrix},\ \begin{pmatrix} u \\ \overline{u} \end{pmatrix} = \begin{bmatrix} 1 & \gamma \\ 1 & -\gamma \end{bmatrix}\begin{pmatrix} u_{x'} \\ u_{y'} \end{pmatrix},$$
$$\begin{pmatrix} \sigma \\ \overline{\sigma} \end{pmatrix} = \begin{bmatrix} A & -\gamma \\ A & \gamma \end{bmatrix}\begin{pmatrix} \sigma_1 \\ \sigma_2 \end{pmatrix}, \tag{A2}$$

as well as of the derivatives $\partial_w = \frac{1}{2}\left(\partial_{x'} + \gamma\partial_{y'}\right)$ and $\partial_{\overline{w}} = \frac{1}{2}\left(\partial_{x'} - \gamma\partial_{y'}\right)$ are needed to express the elasticity problem in the complex formulation. In this form, it turns out that a displacement field does not generate energy contributing components ε_1 and ε_2 is equivalent to requiring that $\partial_{\overline{w}}u = \partial_w\overline{u} = 0$, thus any pair of the analytic displacement field $u = f_1(w)$, $\overline{u} = f_2(\overline{w})$ is stress-free. On the other hand, the equilibrium equation $\nabla_{\mathbf{X}'}\cdot\boldsymbol{\sigma} = 0$ transforms to $\partial_{\overline{w}}\sigma = \partial_w\overline{\sigma} = 0$. Again, a dual consequence holds in that a pair of analytic stress field $\sigma = g_1'(w)$, $\overline{\sigma} = g_2'(\overline{w})$ is allowable. The stress-bearing displacement field can then be obtained by integration of corresponding strain field [25]. The displacement fields of Eqs. (32) and (33) are obtained with $f_1(w) = g_1(w) = w^2 + 2w^3$, $f_2(\overline{w}) = g_2(\overline{w}) = \overline{w}^2 + 2\overline{w}^3$, followed by inverse transformation of Eq. (A2) and coordinate rotation to x-y system.

Author contributions ***Kun Wang:*** *Conceptualization, Formal analysis, Investigation, Methodology, Software, Validation, Visualization, Writing – original draft, Writing – review & editing.* ***Haiyu Lv:*** *Validation, Visualization, Writing – original draft.* ***Xiaoning Liu*** *&* ***Gengkai Hu:*** *Conceptualization, Methodology, Writing – review & editing, Supervision, Funding acquisition.* ***Anfu Zhang:*** *Investigation, validation.*

Acknowledgements *This work was supported by the National Natural Science Foundation of China (Grant Nos. 11972080, 11972083 and 11991030), and the Innovation Foundation of Maritime Defense Technologies Innovation Center (Grant No. JJ-2021-719-06).*

1 G. W. Milton, and A. V. Cherkaev, Which elasticity tensors are realizable? J. Eng. Mater. Tech. **117**, 483 (1995).
2 X. Cai, L. Wang, Z. Zhao, A. Zhao, X. Zhang, T. Wu, and H. Chen, The mechanical and acoustic properties of two-dimensional pentamode metamaterials with different structural parameters, Appl. Phys. Lett. **109**, 131904 (2016).
3 Y. Chen, and G. Hu, Broadband and high-transmission metasurface for converting underwater cylindrical waves to plane waves, Phys. Rev. Appl. **12**, 044046 (2019).
4 Y. Chen, X. Liu, and G. Hu, Design of arbitrary shaped pentamode acoustic cloak based on quasi-symmetric mapping gradient algorithm, J. Acoust. Soc. Am. **140**, EL405 (2016).
5 Y. Chen, M. Zheng, X. Liu, Y. Bi, Z. Sun, P. Xiang, J. Yang, and G. Hu, Broadband solid cloak for underwater acoustics, Phys. Rev. B **95**, 180104 (2017).
6 N. H. Gokhale, J. L. Cipolla, and A. N. Norris, Special transformations for pentamode acoustic cloaking, J. Acoust. Soc. Am. **132**, 2932 (2012).
7 A. C. Hladky-Hennion, J. O. Vasseur, G. Haw, C. Croënne, L. Haumesser, and A. N. Norris, Negative refraction of acoustic waves using a foam-like metallic structure, Appl. Phys. Lett. **102**, 144103 (2013).

8 M. Kadic, T. Bückmann, N. Stenger, M. Thiel, and M. Wegener, On the practicability of pentamode mechanical metamaterials, Appl. Phys. Lett. **100**, 191901 (2012).
9 C. N. Layman, C. J. Naify, T. P. Martin, D. C. Calvo, and G. J. Orris, Highly anisotropic elements for acoustic pentamode applications, Phys. Rev. Lett. **111**, 024302 (2013).
10 A. N. Norris, Acoustic cloaking theory, Proc. R. Soc. A **464**, 2411 (2008).
11 Z. Sun, H. Jia, Y. Chen, Z. Wang, and J. Yang, Design of an underwater acoustic bend by pentamode metafluid, J. Acoust. Soc. Am. **143**, 1029 (2018).
12 M. Zheng, X. Liu, Y. Chen, H. Miao, R. Zhu, and G. Hu, Theory and realization of nonresonant anisotropic singly polarized solids carrying only shear waves, Phys. Rev. Appl. **12**, 014027 (2019).
13 R. F. Almgren, An isotropic 3-dimensional structure with poisson ratio = −1, J. Elasticity **15**, 427 (1985).
14 R. Lakes, Foam structures with a negative Poisson's ratio, Science **235**, 1038 (1987).
15 G. W. Milton, Composite materials with poisson's ratios close to—1, J. Mech. Phys. Solids **40**, 1105 (1992).
16 J. C. Maxwell, L. On the calculation of the equilibrium and stiffness of frames, London Edinburgh Dublin Philos. Mag. J. Sci. **27**, 294 (1864).
17 X. Mao, N. Xu, and T. C. Lubensky, Soft modes and elasticity of nearly isostatic lattices: randomness and dissipation, Phys. Rev. Lett. **104**, 085504 (2010).
18 K. Sun, A. Souslov, X. Mao, and T. C. Lubensky, Surface phonons, elastic response, and conformal invariance in twisted kagome lattices, Proc. Natl. Acad. Sci. USA **109**, 12369 (2012).
19 C. L. Kane, and T. C. Lubensky, Topological boundary modes in isostatic lattices, Nat. Phys. **10**, 39 (2014).
20 T. C. Lubensky, C. L. Kane, X. Mao, A. Souslov, and K. Sun, Phonons and elasticity in critically coordinated lattices, Rep. Prog. Phys. **78**, 109501 (2015).
21 K. Zhang, F. Hong, J. Luo, and Z. Deng, Topological edge state analysis of hexagonal phononic crystals, Acta Mech. Sin. **38**, 421455 (2022).
22 S. Guest, On the determinacy of repetitive structures, J. Mech. Phys. Solids **51**, 383 (2003).
23 X. Mao, and T. C. Lubensky, Maxwell lattices and topological mechanics, Annu. Rev. Condens. Matter Phys. **9**, 413 (2018).
24 M. Czajkowski, C. Coulais, M. van Hecke, and D. Z. Rocklin, Conformal elasticity of mechanism-based metamaterials, Nat. Commun. **13**, 211 (2022).
25 M. Czajkowski, and D. Z. Rocklin, Duality and sheared analytic response in mechanism-based metamaterials, arXiv: 2205.10751v2 (2022).
26 Y. Wei, and G. Hu, Wave characteristics of extremal elastic materials, Extreme Mech. Lett. **55**, 101789 (2022).
27 G. W. Milton, Complete characterization of the macroscopic deformations of periodic unimode metamaterials of rigid bars and pivots, J. Mech. Phys. Solids **61**, 1543 (2013).
28 M. Cai, X. Liu, G. Hu, and P. Zhou, Customization of two-dimensional extremal materials, Mater. Des. **218**, 110657 (2022).
29 Q. Li, Y. Qu, Y. Luo, and S. Liu, Concurrent topology optimization design of stiffener layout and cross-section for thin-walled structures, Acta Mech. Sin. **37**, 472 (2021).
30 N. Wei, H. Ye, X. Zhang, W. Wang, and Y. Sui, Lightweight topology optimization of graded lattice structures with displacement constraints based on an independent continuous mapping method, Acta Mech. Sin. **38**, 421352 (2022).
31 L. Chen, J. Wan, X. Chu, and H. Liu, Parameterized level set method for structural topology optimization based on the Cosserat elasticity, Acta Mech. Sin. **37**, 620 (2021).
32 R. S. Kumar, and D. L. McDowell, Generalized continuum modeling of 2-D periodic cellular solids, Int. J. Solids Struct. **41**, 7399 (2004).
33 X. N. Liu, G. L. Huang, and G. K. Hu, Chiral effect in plane isotropic micropolar elasticity and its application to chiral lattices, J. Mech. Phys. Solids **60**, 1907 (2012).
34 P. G. Martinsson, and I. Babuška, Mechanics of materials with periodic truss or frame micro-structures, Arch. Rational Mech. Anal. **185**, 201 (2007).
35 A. N. Norris, Mechanics of elastic networks, Proc. R. Soc. A **470**, 20140522 (2014).
36 H. Tollenaere, and D. Caillerie, Continuous modeling of lattice structures by homogenization, Adv. Eng. Software **29**, 699 (1998).
37 S. Alexander, Amorphous solids: Their structure, lattice dynamics and elasticity, Phys. Rep. **296**, 65 (1998).
38 R. G. Hutchinson, and N. A. Fleck, The structural performance of the periodic truss, J. Mech. Phys. Solids **54**, 756 (2006).
39 S. Pellegrino, Structural computations with the singular value decomposition of the equilibrium matrix, Int. J. Solids Struct. **30**, 3025 (1993).
40 S. Pellegrino, and C. R. Calladine, Matrix analysis of statically and kinematically indeterminate frameworks, Int. J. Solids Struct. **22**, 409 (1986).
41 M. S. A. Elsayed, and D. Pasini, Comprehensive stiffness of prestressed lattice materials, J. Mater. Sci. Res. **1**, 87 (2012).
42 A. Bossart, D. M. J. Dykstra, J. van der Laan, and C. Coulais, Oligomodal metamaterials with multifunctional mechanics, Proc. Natl. Acad. Sci. USA **118**, e2018610118 (2021).
43 A. Bossart, and R. Fleury, Extreme Spatial dispersion in nonlocally-resonant elastic metamaterials, 2022, arXiv: 10.48550/arXiv.2209.02618.
44 P. Dieleman, N. Vasmel, S. Waitukaitis, and M. van Hecke, Jigsaw puzzle design of pluripotent origami, Nat. Phys. **16**, 63 (2020).

基于桁架格栅的二维模式材料设计方法

王坤, 吕海宇, 刘晓宁, 张安付, 胡更开

摘要 具有不满秩弹性张量的模式材料(extremal material)可以根据其具有的软模式(soft deformation mode或者soft mode)数目进行分类, 其具体的弹性性质则由其硬模式(hard modes)决定. 迄今为止, 只有具有单一硬模式的五模材料得到了深入的研究, 包含其他模式材料的更广阔空间则几乎未被探索. 本文基于桁架格栅, 研究了设计更一般的模式材料的基本工具和设计方案. 为了均匀化具有由局部机构引起的非仿射变形的周期格栅, 我们回顾了奇异值分解的矩阵公式, 并推导了形如开尔文分解的、紧凑形式的有效弹性张量, 由此我们能够概述模式材料的产生机理和设计逻辑. 我们将该方法应用于具有任意指定的弹性张量的二维模式材料的设计. 所设计的格栅材料证实了理想二维一模材料中, 与解析复变函数密切相关的、独特的静态响应. 本文所提出的方法也适用于三维情况下更一般的模式材料.